COMPUTATIONAL ANALYSIS OF MINE BLAST ON A COMMERCIAL VEHICLE STRUCTURE

M. Grujicic[1*], B. Pandurangan[1], I. Haque[1], B. A. Cheeseman[2], W. N. Roy[2] and R. R. Skaggs[2]

[1] *Department of Mechanical Engineering Clemson University, Clemson SC 29634*
[2] *Army Research Laboratory – Survivability Materials Branch Aberdeen, Proving Ground, MD 21005-5069*

Abstract—The kinematic response (including plastic deformation, failure initiation and fracture) of a soft-skinned vehicle (represented by a F800 series single-unit truck) to the detonation of a landmine shallow-buried in (either dry or saturated sand) underneath the vehicle's front right wheel is analyzed computationally. The computational analysis included the interactions of the gaseous detonation products and the sand ejecta with the vehicle and the transient non-linear dynamics response of the vehicle. A frequency analysis of the pressure versus time signals and visual observation clearly show the differences in the blast loads resulting from the landmine detonation in dry and saturated sand as well as the associated kinematic response of the vehicle. It is noted that the dominant vehicle structural response to the blast is similar to the first torsional structural mode shape obtained through an eigenvalue analysis of the system. Tailoring the vehicle modal response may result in more desirable modes of failure.

Keywords: Detonation, Shallow Buried Mine, Blast Loading, AUTODYN

NOMENCLATURE

A	-	Room temperature yield stress
α	-	Porosity
B	-	Compaction Modulus
B_1	-	Strain Hardening Constant
β	-	Saturation ratio
C	-	Strain rate constant
D_{1-5}	-	Constants in Johnson-Cook failure model
E	-	Internal energy
ε	-	Plastic strain
G	-	Shear modulus
γ	-	Constant-Pressure to constant-volume specific heats ratio

---
* E-mail: mica.grujicic@ces.clemson.edu
  Tel: (864) 656-5639, Fax: (864) 656-4435,

		Form Approved
	Report Documentation Page	*Form Approved* *OMB No. 0704-0188*

Public reporting burden for the collection of information is estimated to average 1 hour per response, including the time for reviewing instructions, searching existing data sources, gathering and maintaining the data needed, and completing and reviewing the collection of information. Send comments regarding this burden estimate or any other aspect of this collection of information, including suggestions for reducing this burden, to Washington Headquarters Services, Directorate for Information Operations and Reports, 1215 Jefferson Davis Highway, Suite 1204, Arlington VA 22202-4302. Respondents should be aware that notwithstanding any other provision of law, no person shall be subject to a penalty for failing to comply with a collection of information if it does not display a currently valid OMB control number.

1. REPORT DATE **2007**	2. REPORT TYPE	3. DATES COVERED **00-00-2007 to 00-00-2007**

4. TITLE AND SUBTITLE **Computational Analysis of Mine Blast on a Commercial Vehicle Structure**	5a. CONTRACT NUMBER
	5b. GRANT NUMBER
	5c. PROGRAM ELEMENT NUMBER
6. AUTHOR(S)	5d. PROJECT NUMBER
	5e. TASK NUMBER
	5f. WORK UNIT NUMBER
7. PERFORMING ORGANIZATION NAME(S) AND ADDRESS(ES) **Celmson University,Department of Mechanical Engineering,Clemson,SC,29634**	8. PERFORMING ORGANIZATION REPORT NUMBER
9. SPONSORING/MONITORING AGENCY NAME(S) AND ADDRESS(ES)	10. SPONSOR/MONITOR'S ACRONYM(S)
	11. SPONSOR/MONITOR'S REPORT NUMBER(S)

12. DISTRIBUTION/AVAILABILITY STATEMENT
Approved for public release; distribution unlimited

13. SUPPLEMENTARY NOTES

14. ABSTRACT

The kinematic response (including plastic deformation, failure initiation and fracture) of a soft-skinned vehicle (represented by a F800 series single-unit truck) to the detonation of a landmine shallow-buried in (either dry or saturated sand) underneath the vehicle?s front right wheel is analyzed computationally. The computational analysis included the interactions of the gaseous detonation products and the sand ejecta with the vehicle and the transient non-linear dynamics response of the vehicle. A frequency analysis of the pressure versus time signals and visual observation clearly show the differences in the blast loads resulting from the landmine detonation in dry and saturated sand as well as the associated kinematic response of the vehicle. It is noted that the dominant vehicle structural response to the blast is similar to the first torsional structural mode shape obtained through an eigenvalue analysis of the system. Tailoring the vehicle modal response may result in more desirable modes of failure.

15. SUBJECT TERMS

16. SECURITY CLASSIFICATION OF:			17. LIMITATION OF ABSTRACT	18. NUMBER OF PAGES	19a. NAME OF RESPONSIBLE PERSON
a. REPORT **unclassified**	b. ABSTRACT **unclassified**	c. THIS PAGE **unclassified**	**Same as Report (SAR)**	**30**	

Standard Form 298 (Rev. 8-98)
Prescribed by ANSI Std Z39-18

γ_1	-	Saturation Parameter
Γ	-	Gruneisen parameter
K	-	Bulk Modulus
μ	-	Compression ratio
μ_1	-	Yield-Stress-to-Pressure Proportionality Coefficient
P	-	Pressure
ρ	-	Density
σ	-	Yield Stress
T	-	Temperature
v	-	Specific volume
x	-	Spatial coordinate
y	-	Spatial coordinate
Y	-	Yield stress

Subscripts

$Comp$	-	Value at full compaction
dry	-	Dry Sand quantity
$melt$	-	Melting point quantity
0	-	Initial value
p	-	Pore related quantity
pl	-	Plastic state quantity
$Pl.Comp$	-	Plastic Compaction related quantity
$room$	-	Room temperature quantity
s	-	Fully-compacted sand related quantity
$Solid.Comp$	-	Solid Compaction related quantity
H	-	Homologous quantity
sat	-	Saturation related quantity
$unsat$	-	Unsaturated Sand related quantity
w	-	Water related quantity

Superscripts

$*$	-	Value at minimum pressure for full sand compaction
m	-	Thermal softening exponent
n	-	Strain hardening exponent

I. Introduction

It is well established that light-armored and soft-skinned vehicles are highly vulnerable to anti-vehicular mine blasts [e.g.1]. Traditionally, extensive experimental test programs are employed during the development of anti-mine protection systems aimed at reducing the vulnerability of vehicles and vehicle occupants to mine blasts. Such experimental programs are necessary to ensure the utility and effectiveness of the anti-mine protection systems. However, the use of the experimental programs is typically expensive, time-consuming, involves destructive testing of the vehicles and is generally limited to

vehicles that were already damaged beyond repair or phased out of service. Experimental testing of vehicles currently being produced or under development is often cost prohibitive.

The development of effective mine protection systems for light-armored and soft-skinned vehicles requires a comprehensive understanding of two distinct groups of phenomena: (a) detonation of high-energy explosive mines buried in soil, interaction of the detonation products with surrounding soil and interaction of mine blast fragments, gaseous detonation products and soil ejecta with target vehicle/structures; and (b) the structural/ballistic response of the target vehicle/structure subjected to transient highly-nonlinear dynamic/impulse loading resulting from the mine blast. While the role of experimental test programs remains critical in elucidating the nature of the aforementioned phenomena, they are increasingly being complemented and partly substituted with the corresponding computation-based engineering analyses.

In recent years, major advances have been made in modeling the detonation phenomena, the constituent response of the materials under high deformation-rate, large-deformation, ballistic conditions and the interactions between detonation products, soil and target vehicles/structures. In particular, these models have enabled the coupling between Eulerian representations (typically applied to the gaseous detonation products and air) and Lagrange representations (typically applied to the target vehicles/structure, mine-casing fragments and soil). These advances in the modeling of the phenomena accompanying detonation of a shallow-buried mine in the vicinity of a target vehicle/structure combined with the major advances in the computational software and hardware has enabled the computational engineering analyses, as mentioned earlier, to be used to complement and often substitute extensive experimental testing [2,3].

To the author's best knowledge, all the computational analyses reported in the open literature and pertaining to the phenomena accompanying the detonation of a shallow-buried mine in the vicinity of a target vehicle/structure emphasize one of the following: (a) An accurate modeling of mine detonation, interactions between the detonation products and the surrounding soils and the determination of the spatial and temporal evolutions of the resulting specific impulse [e.g. 4,5]; (b) An accurate quantification of the interactions between the mine-blast waves and the (rigid and stationary) target vehicle/structures [e.g. 6]; and (c) A detailed numerical analysis of the structural and ballistic response of the target vehicle/structure when subjected to (simplified empirically-based) mine-blast induced impulse loading [e.g. 2,3]. All these analyses suffer from serious limitations. For example, in the analyses of type (a), no interactions between mine-casing fragments, detonation products and soil ejecta, on one hand, and the target vehicle/structure, on the other, are considered. Such interactions are considered in the analyses of type (b), but the target vehicle/structure is not allow deflecting or moving and only provides rigid and stationary walls which define a spatial region within which the gaseous detonation products are confined. In the analyses of type (c), the structural response of the target vehicle/structure is enabled but the interactions between the gaseous detonation products, soil ejecta and the target vehicle/structure is oversimplified by replacing them with empirically-based relations for the initial velocity or the impulse force.

The objective of the present work is to develop the basic frame work for combining computational fluid dynamics (used to model the behavior of gaseous detonation products and air) with the computational structural dynamics (used to model the soil and

the target vehicle/structures) in order to gain more insight into the complex phenomena accompanying detonation of a shallow-buried mine in the vicinity of a vehicle. This approach has been applied to the case of a Ford F800 series single-unit truck (representative of a soft-skinned multipurpose transport vehicle) subjected to the blast loading resulting from the detonation of a 7.5kg anti-vehicle mine shallow-buried in (either dry or fully saturated) soil and detonated underneath the front right wheel of the vehicle.

The organization of the paper is as follows. A brief description of the use of transient non-linear dynamics in modeling the interactions between mine-detonation products, soil and target vehicle/structure is presented in Section II.1. The problem definition, geometrical models for the vehicle, mine, soil and air, the mechanical materials models and details of the computational procedure used are all discussed in Section II.2. The results obtained in the present work are presented and discussed in Section III. The main conclusions resulting from the present work are summarized in Section IV.

II. COMPUTATIONAL PROCEDURE

II.1. Transient Non-linear Dynamics Modeling

All the calculations carried out in the present work were done using AUTODYN, a general purpose transient non-linear dynamics analysis software [7]. In our previous work [8], a detailed account was provided of the basic features of AUTODYN, emphasizing the ones which are most relevant for modeling detonation of shallow-buried and ground-laid mines and the subsequent interactions between detonation products, soil ejecta and target vehicle/structure. Therefore, only a brief overview of AUTODYN is given in this section.

A transient non-linear dynamics problem such as the interactions between shallow-buried mine detonation products and soil ejecta with the target vehicle/structure is analyzed within AUTODYN by solving simultaneously the governing partial differential equations for the conservation of momentum, mass and energy along with the material constitutive equations and the equations defining the initial and the boundary conditions. The aforementioned equations are solved numerically using a second-order explicit scheme. Due to the large motions and deformations of the detonation products and air these materials are analyzed using an Euler control-volume computational scheme (the computational grid is fixed in space and time while the material(s) move through it). On the other hand, the soil and target vehicle/structure are analyzed using a Lagrange scheme (the computational grid is tied to the material and moves and deforms with it).

The interactions between different components/materials as well as self-interactions can be analyzed in AUTODYN using various Lagrange-Lagrange and Euler-Lagrange coupling options and impact/slide interaction algorithm. A detailed overview of these options was given in our previous work [8].

II.2 Problem Definition and Computational Analysis

In this section, a brief description is given of the computational analysis used to simulate the interactions between the detonation-products/soil ejecta resulting from the explosion of a shallow-buried mine and the Ford F800 single-unit truck. The computational

modeling of these interactions involved two distinct steps: (a) geometrical modeling of the F800 series truck along with the adjoining mine, air and sand regions, and (b) the associated transient non-linear dynamics analysis of the impulse loading (momentum transfer) from the detonation-products/soil ejecta to the vehicle structure.

II.2.1. Geometric Model for Ford F800 Series Single-Unit Truck

The finite element model of a Ford F800 series truck (representative of a soft-skinned single-unit multipurpose transport vehicle) was developed at the NCAC (National Crash Analysis Center) for the Federal Highway Administration (FHWA) and the National Highway Traffic Safety Administration (NHTSA) [9]. The main design characteristics of a Ford F800 series truck are as follows: (a) a parallel-rail frame type chassis; (b) leaf springs based front and rear suspension systems; (c) a V-8 diesel or gasoline engine; (d) dual wheel rear axles; (e) cargo body mounted on a series of lateral C- or I-beams welded to C-channels that run parallel and directly atop the chassis main frames; (f) a wooden member between the parallel C-channels and the chassis frame rails; (g) large U-bolts fastening cargo C-channels to chassis main rails; (h) an overall length of 8.582m and a wheelbase of 5.148m and (i) an empty weight of 5214kg. A summary of the vehicle parts is given in Table 1.

The truck was first disassembled at the NCAC into 147 components (in many cases each component (e.g. engine) consisted of many parts). The three dimensional geometry data for each part was then obtained by using a passive digitizing arm connected to a computer based data acquisition system. The surface patches generated from specified digitized data were the stored in AUTOCAD in the IGES format. These IGES files were then imported into PATRAN [10] for mesh generation and model assembly. The model was then translated from PATRAN, which outputs a neutral file, into LS-DYNA3D [11] input file using a translator called HPD [12] developed at NCAC. This LS-DYNA3D input file (developed at NCAC) is next imported, in the present work, to AUTODYN, a transient nonlinear dynamics simulation package [7]. Since the model was previously used for vehicle-crash simulation, considerable detail was given to the rail frame, front structures (including bumper), radiator, radiator assembly, door and cabin of the vehicle. These parts were digitized as detailed as possible, minimizing any loss of part's geometry. The finite element model for the F800 series truck as used in the present work is shown in Fig.1. The model consists of 147 components, 24915 nodes, 1492 eight-node solid elements, 10109 four-node shell elements and 124 two-node beam elements. Adjacent components are connected using one of the following three ways: (a) node sharing; (b) using nodal constraint option such as constrained nodal rigid bodies (a group of nodes is treated as a rigid body) and using spot welds (two nodes connected using a rigid beam, these nodes translate and rotate together) and (c) spherical and revolute joints (front suspension parts).

Table 1 Names and Descriptions of the Parts Used in the Finite Element Analysis of the Ford F800 Series Single Unit Truck.

Part Name	No. of Parts	Part Description/Function
Tires, Wheel, Steering and Braking (Front)		
Tire Tread	2	Provides a better traction with the road
Tire Walls	2	Walls of the tire

Rims	2	Connect the tire to the brake assembly
Spokes Thin	2	Support the tire rims
Spokes Thick	2	Support the tire rims
Spokes Solid	2	Support the tire rims
Axis Beam	2	Connects the wheel assembly to the front axle
Disk Brake System	2	A simple model for the disc-type brake system
Brake Discs	4	A simple model of the brake disc
Axle	1	connects the wheel assembly to the suspension
Tires, Wheel and Braking (Rear)		
Outer Tire Treads	2	Provides a better traction with the road
Inner Tire Treads	2	Provides a better traction with the road
Outer Tire Walls	2	Walls of the outer tire
Inner Tire Walls	2	Walls of the inner tire
Brake Rims	3	Connect the tire to the brake assembly
Rim Beam	2	Connects the tire rim to the rear axle
Rim Hinge	2	Connects the rear axle to the wheel assembly
Suspension (Front)		
Leaf Springs	11	Leaf suspension-system springs
Spring Connector Rod 1	2	Connect the springs to the U-connectors
Spring Connector Rod 2	2	Connect the springs to the U-connectors
Spring Support	1	Support the springs
U-shape Connectors	4	Connect the springs to the main rails
Dampers/Shock Absorbers	1	Absorbs shock and dampens vibrations
Suspension (Rear)		
Upper Leaf Springs	7	Upper leaf suspension-system springs
Spring Connector Rods	4	Connect the springs to the U-connectors
Limiters	4	Limits spring travel
Main Spring	1	Main leaf suspension-system spring
Lower Springs	2	Lower leaf suspension-system springs
Chassis		
Bumpers	2	Prevent low-velocity impact damage
Main Rails	2	Provide longitudinal bending/torsional stiffness
Bed Rail	1	Beam support structure for the cargo compartment
Support Rail	4	Side members supporting the main rails
Cross Members	3	Provide transverse connect between main rails
Stiffening Beams	2	Connect the cargo compartment to the bed rail
Support Beams	2	Provide support for the fuel tank
Uprights	2	Connect the front and rear axles to the wheel assembly
Engine, A/C, Radiator, Batteries and Tank		
Engine	1	Provides the power to the vehicle
Engine-mount Cross Member	1	Connect main rails for engine support
Engine-mount Beam	1	Connects engine to the cross-member
Radiator Assembly	4	A simple model for the radiator /cooling system
Batteries	1	A simple model of the auxiliary power system
Fuel Tank	1	Holds fuel

Transmission		
Gear Box	1	Encloses the gears and the primary transmission parts
Transmission Joints	8	Connect the different parts of the transmission system
Shaft Members	3	Drive train members
Differential	2	Enables differential wheel speeds
Bearing/Suspension	1	Provides support for the drive train shafts
Body		
Cabin	2	A simple model of the driver compartment
Cabin Suspension	2	Provides support to the driver compartment
Stair	1	Aids in mount and dismount from the vehicle
Door	2	A simple model of the cabin door
Hood	2	Provides upper closure to the engine compartment
reinforcing Member	1	Act as reinforcing frames for the cabin
Fender	1	Provide side enclosure to the engine compartment
Wheel House	1	Provide lower enclosure for the engine compartment
Firewall	1	Provides the isolation of the cabin from the engine
Floor	1	Provides lower enclosure for the cabin
Bed Shell	1	A simple model for the cargo compartment
Added Mass	1	Mass added to obtain the correct overall vehicle weight
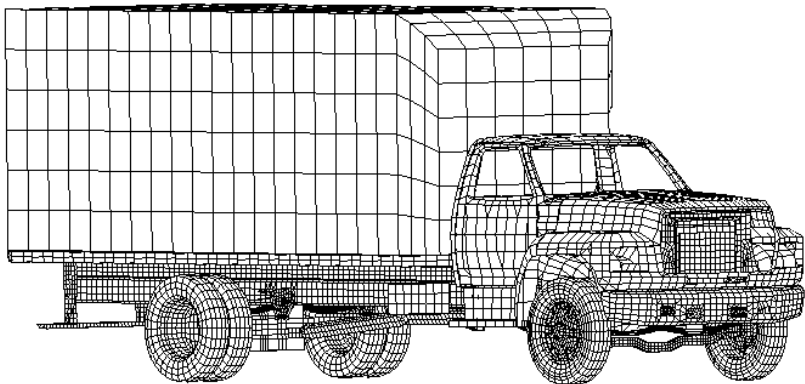
Fig.1 Geometrical model for Ford F800 series single-unit truck [9].

Two classes of materials were assumed to be used in the construction of the Ford F800 series truck: steel (of various grades) and rubber. The tires were assumed to be composed of rubber. The components of the transmission, suspension, braking and steering systems were assumed to be made of AISI 4340 steel. The remaining components of the vehicle were taken to be made of one of the two mild steel grades

with an initial yield stress of 270MPa and 350MPa, respectively. A detailed account of the models used to represent the structural and the ballistic response of these materials is presented in Section II.2.3.

II.2.2. Geometric Model for the Mine, Sand and Air

The computational domain containing the shallow-buried mine, soil and air is modeled following the procedure proposed by Fairlie and Bergeron [13]. This procedure couples a Lagrangian mesh, which is used to model the soil and the target vehicle/structure, to an Euler-FCT mesh, which models the rapidly expanding blast gases and the (initially stationary) air. The Euler-FCT (Flux-Corrected Transport) scheme is a single-material computational scheme which is computationally very efficient in comparison to the Euler multi-material scheme [7]. In the present work, the Euler-FCT scheme is used to model gaseous high-energy, high-pressure detonation products and the ambient air as a single material. The Euler –FCT mesh comprises of two regions, a lower region that overlaps with the soil and an upper region that extends above the soil and encompasses a portion of the vehicle around its front right wheel.

The lower Euler-FCT domain located within the soil contains a region of pressurized air to represent the blast gas products (denoted as "mine" in Fig. 2). The upper Euler-FCT domain is assigned standard (ambient) air properties. The material models used for air, soil and the target vehicle/structure will be reviewed in the next section.
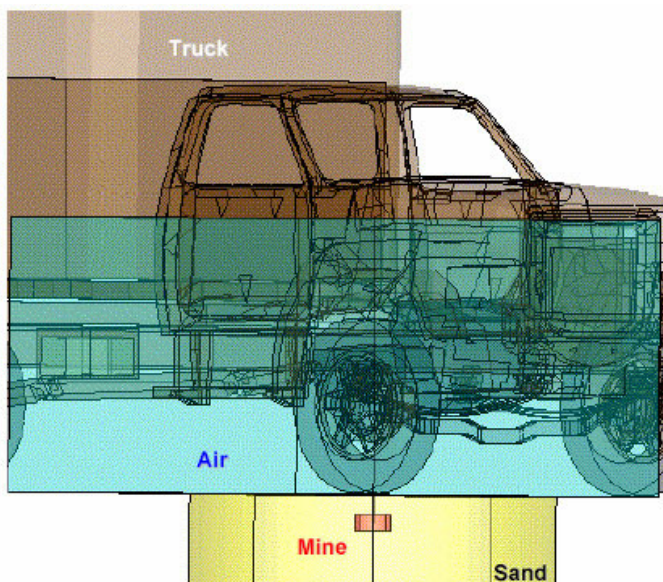
Fig. 2 Geometrical model for mine, sand and surrounding air.

II.2.3   Material Constitutive Models

As discussed in the Section II.1, the complete definition of a transient non-linear dynamics problem entails the knowledge of the material models that define the

relationships between the flow variables (pressure, mass-density, energy-density, temperature, etc.). These relations typically involve an equation of state, a strength equation and a failure equation for each constituent material. These equations arise from the fact that, in general, the total stress tensor can be decomposed into a sum of a hydrostatic stress (pressure) tensor (which causes a change in the volume/density of the material) and a deviatoric stress tensor (which is responsible for the shape change of the material). An equation of state then is used to define the corresponding functional relationship between pressure, mass density and internal energy density (temperature), while a strength relation is used to define the appropriate equivalent plastic strain, equivalent plastic strain rate, and temperature dependencies of the equivalent deviatoric stress. In addition, a material model generally includes a failure criterion, i.e. an equation describing the (hydrostatic or deviatoric) stress and/or strain condition(s) which, when attained, causes the material to fracture and lose its ability to support (abruptly in the case of brittle materials or gradually in the case of ductile materials) normal and shear stresses.

In the present work, the following materials are utilized within the computational domain: air, various grades of steel, rubber and soil. In the following sections, a brief description is given of the models used for these constituent materials. The values of all the material parameters for air and the various grades of steel are available in the AUTODYN materials library [11]. The values of the material parameters for rubber are given later in this section. The material model parameters for soil can be found in our recent work [4].

Air

Air is modeled as an ideal gas and, consequently, its equation of state is defined by the ideal-gas gamma-law relation as [7]:

$$P = (\gamma - 1)\frac{\rho}{\rho_0}E \qquad (1)$$

where P is the pressure, γ the constant-pressure to constant-volume specific heats ratio (=1.4 for a diatomic gas like air), ρ_0 (=1.225kg/m^3) is the initial air mass density, and ρ is the current density. For Eq. (1) to yield the standard atmosphere pressure of 101.3kPa, the initial internal energy density E is set to 253.4kJ/m^3 which corresponds to the air mass specific heat of 717.6J/kg·K and a reference temperature of 288.2K.

Due to the use of a single-material Euler-FCT processor for the gas-phase region, the landmine detonation products are not modeled as a separate material within the gas phase. Rather, the landmine detonation products are modeled initially as a cylindrically shaped air region with a high density ρ and a high internal energy density. Following Fairlie [13], the initial density of the detonation products is taken to be the density of the solid C4 explosive and the initial internal energy of this gas is determined by converting the value of the Chapman-Jouget internal energy per unit volume to the corresponding value of the internal energy per unit mass. The corresponding detonation products pressure and the fire ball temperature are computed using standard thermodynamic relations.

Since air is a gaseous material and has no ability to support either shear stresses or negative pressures, no strength or failure relations are required for this material.

Steel

In the present work, with the exception of the tires all the components of the Ford F800 series single-unit trucks are assumed to be made of various grades of steel. For all these grades of steel, a linear type of equation of state was used which assumes a Hooke's law type relationship between the pressure and the volume change as:

$$P = K\mu \tag{2}$$

where K is the bulk modulus of the material and $\mu = \left(\dfrac{\rho}{\rho_o} - 1 \right)$ is the compression ratio (ρ is the current material mass-density). Within the AUTODYN material database, the initial material density ρ_o, the bulk modulus K, the specific heat and the reference temperature are defined for the various grades of steel.

To represent the constitutive response of the steels under deviatoric stress, the Johnson-Cook Strength model [14] is used. This model is capable of representing the material behavior displayed under large-strain, high deformation rate, high-temperature conditions, of the type encountered in problems dealing with the interactions of detonation products and solid structures. Within the Johnson-Cook strength model, the yield stress is defined as:

$$Y = \left[A + B\varepsilon_{pl}^n \right]\left[1 + C \log \dot{\varepsilon}_{pl} \right]\left[1 - T_H^m \right] \tag{3}$$

where ε_{pl} is the equivalent plastic strain, $\dot{\varepsilon}_{pl}$ is the equivalent plastic strain rate, A is the zero plastic strain, unit plastic strain rate, room temperature yield stress, B is the strain hardening constant, n is the strain hardening exponent, C is the strain rate constant, m is the thermal softening exponent and $T_H = (T-T_{room})/(T_{melt}-T_{room})$ is a room temperature (T_{room}) based homologous temperature while T_{melt} is the melting temperature. All temperatures are given in Kelvin.

Since all the grades of steel considered in the present work exhibit a ductile model of failure, their failure condition was defined using the Johnson-Cook failure model [15]. The progress of failure according to the Johnson-Cook failure model is defined by the following cumulative damage law:

$$D = \sum \frac{\Delta\varepsilon}{\varepsilon_f} \tag{4}$$

where $\Delta\varepsilon$ is the increment in effective plastic strain with an increment in loading and ε_f, is the failure strain at the current state of loading which is a function of the mean stress, the effective stress, the strain rate and the homologous temperature, given by:

$$\varepsilon_f = \left[D_1 + D_2 \exp(D_3\sigma^*) \right]\left[1 + D_4 \ln \dot{\varepsilon}_{pl} \right]\left[1 + D_5 T_H \right] \tag{5}$$

where σ^* is mean stress normalized by the effective stress. The parameters D_1, D_2, D_3, D_4 and D_5 are all material specific constants. Failure is assumed to occur when $D=1.0$.

Rubber

The mechanical response of rubber (the material used for tires) was represented using the extended Blatz-Ko material model. Within the model, a linear equation of state of

the form given by Eq. (2) is used. The material is farther assumed to be fully elastic with an initial shear modulus of 42.3GPa. The Blatz-Ko model [16] used is a special form of the hyper-elastic material response obtained in elastomers. In these materials, the relationship between the (2nd Piola-Kirchhoff) stress and (Green-Lagrange) strain is given by a strain energy density function, which depends only on strain invariants. The definition of the strain energy function typically requires the knowledge of only few parameters (only one, the initial shear modulus in the case of the Blatz-Ko rubber model).

Since the front right tire, which is located right above the mine, is expected to rupture after mine detonation, a simple failure model is used to extend the Blatz-Ko rubber model. This model is based on a (geometrical) failure strain whose magnitude was set to a value 5.0.

Soil

Soil has generally a complex structure consisting of mineral solid particles which form a skeleton. The pores between the solid particles are filled with a low-moisture air (this type of sand is generally referred to as *"dry sand"*), with water containing a small fraction of air (*"saturated sand"*) or comparable amounts of water and air (*"unsaturated sand"*). The relative volume fractions of the three constituent materials in the soil (the solid mineral particles, water and air) are generally quantified by the porosity, α, and the degree of saturation (Saturation Ratio), which are respectively defined as

$$\alpha = \frac{V_p}{V} \tag{6}$$

and

$$\beta = \frac{V_w}{V_p} \tag{7}$$

where V_p is the volume of void (pores), V_w is the volume of water and V is the total volume.

The mechanical response of soil is represented in the present work using the modified compaction material model for soil proposed in our recent work [4]. This model accounts for the effect of moisture content on the behavior of soil. Within the model separate relationships are derived for dry and saturated soil and the corresponding relationship for unsaturated soil (soil with a degree of saturation between 0.0 and 1.0, exclusive) is obtained using appropriate combination of the dry and saturated soil relationships.

Within the equation of state, two types of relationships are defined: (a) density dependence of pressure; and (b) density dependence of sound speed.

The pressure vs. density behavior of dry soil is represented using the original compaction model, as proposed by Laine and Sandvik [17], in the form:

$$P_{dry} = \begin{cases} 0 & \rho_{dry} \leq \rho_{o,dry} \\ B_{Pl.Comp}\left(\rho_{dry} - \rho_{o,dry}\right) & \rho_{o,dry} \leq \rho_{dry} \leq \rho_{dry}^* \\ B_{SolidComp}\left(\rho_{dry} - \rho_s\right) & \rho_{dry} > \rho_{dry}^* \end{cases} \tag{8}$$

where $B_{Pl.Comp}$ and $B_{SolidComp}$ (=21.68 MPa.m^3/kg) are respectively the plastic compaction (densification) and the solid-particle compaction moduli, while $\rho_{o,dry} = (1 - \alpha_o)\rho_s$ and ρ_s (=2641 kg/m^3) are the initial density of dry sand and the density of the fully compacted sand, respectively and α_o denotes the initial porosity in sand. It should be noted, that the compaction moduli used in Eq.(8) are defined as a ratio of the corresponding bulk moduli and mass-densities. The plastic compaction modulus, $B_{Pl.Comp}$, is defined as:

$$B_{Pl.Comp} = \frac{P_{Comp}}{\left(\rho_{dry}^* - \rho_{o,dry}\right)} \tag{9}$$

where P_{Comp} (=0.6506GPa) is the minimum pressure needed for full densification of sand and ρ_{dry}^* is given by;

$$\rho_{dry}^* = \rho_s + \frac{P_{Comp}}{B_{SolidComp}} \tag{10}$$

The pressure vs. density curve for saturated soil is taken to be rate independent and to correspond to the P vs. ρ relationship associated with a (high) deformation rate. The relationship can be expressed as:

$$P_{sat} = \begin{cases} 0 & \rho_{sat} \leq \rho_{o,sat} \\ B_{Sat}(\rho_{sat} - \rho_{o,sat}) & \rho_{sat} > \rho_{o,sat} \end{cases} \tag{11}$$

where B_{Sat} is the compaction modulus of saturated sand and is defined using the compaction modulus of solid particles, $B_{SolidComp}$ and the compaction modulus of water, B_w, and the fact that both the solid phase and the water-filled porosity form continuous networks, as:

$$B_{Sat} = (1 - \alpha)B_{SolidComp} + \alpha B_w \tag{12}$$

while $\rho_{o,sat}$ is the initial density of saturated soil and is defined in terms of the density of solid mineral particles, ρ_s, and the density of water, ρ_w, as:

$$\rho_{o,sat} = (1 - \alpha_o)\rho_s + \alpha_o \rho_w \tag{13}$$

The pressure vs. density curve for unsaturated soil is obtained as a linear combination of the pressure vs. density relations for the dry and the saturated soils, as:

$$P_{unsat}(\alpha_o, \beta) = \begin{cases} 0 & \rho_{unsat} \leq \rho_{o,unsat} \\ B_{unsat,low}(\rho_{unsat} - \rho_{o,unsat}) & \rho_{o,unsat} \leq \rho_{unsat} \leq \rho_{unsat}^* \\ B_{unsat,high}(\rho_{unsat} - \rho_{unsat}^*) & \rho_{unsat} > \rho_{unsat}^* \end{cases} \tag{14}$$

where

$$\rho_{o,unsat} = (1 - \beta)\rho_{o,dry} + \beta \rho_{o,sat} \tag{15}$$

$$\rho_{unsat}^* = (1 - \gamma_1)\rho_{dry}^* + \gamma_1 \rho_{sat}^{*(P=P_{Comp})} \tag{16}$$

$$B_{unsat,low} = \frac{P_{Comp}}{\left(\rho^*_{unsat} - \rho_{o,unsat}\right)} \tag{17}$$

$$B_{unsat,high} = \left[\frac{1}{\dfrac{(1-\beta)}{B_{SolidComp}} + \dfrac{\beta}{B_{Sat}}}\right] \tag{18}$$

where

$$\gamma_1 = \beta\left[\frac{1 - \dfrac{P_{Comp}}{B_{Sat}\rho^*_{sat}}}{(1-\beta)\left(1 - \dfrac{P_{Comp}}{B_{Pl.Comp}\rho^*_{dry}}\right) + \beta\left(1 - \dfrac{P_{Comp}}{B_{Sat}\rho^*_{sat}}\right)}\right] \tag{19}$$

Eq. (18) reflects the fact that the compaction modulus of humid air residing in soil, consisting of dry air and water, is dominated by its more compliant phase (dry air).

In addition to specifying the pressure vs. density relation, the compaction model for soil entails the knowledge of the density dependence of the material's sound speed. The material sound speed is defined as a square-root of the ratio of the bulk modulus and the material mass density. The original compaction model for sand uses the following relation for the density-dependent bulk modulus for dry soil:

$$K_{dry} = \begin{cases} 0 & \rho_{dry} < \rho_{o,dry} \\ -15.6302 + 0.0094074\rho_{dry} & \rho_{o,dry} < \rho_{dry} \leq 0.8137\rho_s \\ -93.05 + 0.0455\rho_{dry} & 0.8137\rho_s \leq \rho_{dry} \leq 0.9837\rho_s \\ -1873.3 + 0.73074\rho_{dry} & 0.9837\rho_{dry} < \rho_{dry} < \rho_s \\ -3.233 + 0.022651\rho_{dry} & \rho_{dry} > \rho_s \end{cases} \tag{20}$$

The density-dependent bulk modulus in saturated soil is derived following the same procedure as in the case of P_{sat} vs. ρ_{sat} relation as:

$$K_{sat} = B_{sat}\rho_{sat} \tag{21}$$

Likewise, the density-dependent bulk modulus for unsaturated soil is defined as:

$$K_{unsat}(\rho_{unsat}, \alpha_o, \beta) = \left[\frac{1}{\dfrac{(1-\beta)}{K_{dry}(\rho_{dry})} + \dfrac{\beta}{K_{sat}(\rho_{sat})}}\right] \tag{22}$$

where

$$\rho_{dry} = \rho_{unsat} - \alpha_o\beta\rho_w \tag{23}$$

and

$$\rho_{sat} = \rho_{unsat} + \alpha_o(1-\beta)\rho_w \tag{24}$$

As mentioned earlier, the density dependent sound speed (for dry, saturated and unsaturated soils) is defined as a square root of the ratio of the corresponding bulk moduli and mass densities.

Within the original compaction strength model for dry soil the pressure dependence of yield stress is defined as:

$$\sigma_{y,dry} = \mu_{1\,dry}P_{dry} \approx \begin{cases} 1.3732P_{dry} & 0 < P_{dry} \leq P_{MC} \\ 1.3732P_{MC} & P_{dry} > P_{MC} \end{cases} \tag{25}$$

Also for the saturated soil, as discussed in our previous work [4], the pressure-dependent yield stress can be defined as:

$$\sigma_{y,sat} = \begin{cases} \mu_{1\,sat}P_{sat} & 0 \leq P_{sat} \leq P_{MC} \\ \mu_{1\,sat}P_{MC} & P_{sat} > P_{MC} \end{cases} \tag{26}$$

where the yield-stress-to-pressure proportionality coefficient, μ_{1sat}, is defined as:

$$\mu_{1\,sat} = \begin{cases} \sqrt{3}\left(0.1 + \dfrac{1.2}{\sqrt{3}}\dfrac{P_{sat}}{P_{MC}}\right) & 0 \leq P_{sat} \leq P_{MC} \\ 1.3732 & P_{sat} > P_{MC} \end{cases} \tag{27}$$

The term P_{MC} (=1.864e5 kPa) appearing in Eqs.(25)- (27) is the Mohr-Coulomb pressure beyond which the yield stress is pressure insensitive.

The yield stress vs. pressure relationship for the unsaturated soil can then be defined using a linear combination of the yield-stress/pressure proportionality coefficients in dry and the saturated soils as:

$$\sigma_{y,sat} = \begin{cases} \mu_{1un\,sat}P_{unsat} & 0 \leq P_{unsat} \leq P_{MC} \\ \mu_{1un\,sat}P_{MC} & P_{unsat} > P_{MC} \end{cases} \tag{28}$$

where

$$\mu_{1unsat} = (1-\beta)\mu_{1\,dry} + \beta\mu_{1\,sat} \tag{29}$$

In addition to specifying the yield stress vs. pressure relationship, the compaction strength model entails the knowledge of the density dependent shear modulus. Since water has no ability to support shear stresses, the shear modulus, G, of unsaturated soil is dominated by the shear modulus of the solid skeleton of the soil. However, the presence of water changes the density of the soil. Therefore, the original compaction shear modulus vs. density relationship defined (using ten pairs of (G, ρ) points in AUTODYN) had to be modified in our previous work [4] by adding a term $\alpha\beta\rho_w$ to the values of density in order to obtain a (deformation-rate independent) shear modulus vs. density relationship for unsaturated soil, thus:

$$\rho_{unsat} = \rho_{dry} + \alpha\beta\rho_w \tag{30}$$

It is well established that the presence of moisture in soil increases the soil's cohesive strength [18]. Therefore, the magnitude of the (negative) failure pressure for soil is expected to increase with the saturation ratio (β). Also, the moisture content should be

substantial (β>0.7) before its effect on the cohesive strength of soil becomes significant [18]. To account for these two observations, the following expression was proposed in our previous work [4] for the magnitude of the (negative) failure pressure in unsaturated soil; $P_{fail,unsat}$:

$$P_{fail,unsat} = \beta^5 P_{fail,sat} \tag{31}$$

where $P_{fail,sat}$ (set equal to 729kPa) is the failure pressure in saturated soil [18]. The relationship given by Eq. (31) correctly predicts that the cohesive strength of unsaturated soil with a saturation ratio of 0.7 is around 10-15% of that in the saturated soil.

II.2.4 Numerical Solution of the Problem

In this section, a brief description is given of the computational analysis used to simulate the interaction of the detonation-products/soil ejecta resulting from the explosion of a shallow-buried mine with the Ford F800 series single –unit truck. The case of a 7.5kg C4 mine with a circular disc shape, a radius of 0.203m and a height of 0.147m and buried in soil to a depth of 0.1m underneath the front right tire of the truck is considered. Details regarding the geometry of the vehicle, mine and the soil and the material models used were given in Section II.2.1, II.2.2 and II.2.3, respectively.

The air/soil and air/vehicle interactions were accounted for using the appropriate Euler-Lagrange coupling option within AUTODYN [7]. Likewise, the sand/vehicle interactions were modeled through the use of the appropriate Lagrange-Lagrange coupling option.

The "*flow out*" boundary conditions were applied to all the free faces (the faces which do not represent interfaces between the different domains) of the Euler-FCT domain. To reduce the effect of reflection of the shock waves at the outer surfaces of the Lagrange soil domain, "*transmit*" boundary conditions were applied to all the free faces of this domain except for the upper face which defines the soil/air and soil/vehicle interfaces. The transmit boundary conditions enable the propagation of pressure waves across the boundaries without reflection, mimicking wave propagation in an infinitely-large soil domain [7].

Several gage points were defined within the landmine, soil, air and the vehicle which allowed monitoring of the quantities such as pressure, velocity and (in the case of the Lagrange domains) of the vertical displacements.

At the beginning of the simulation, all the Lagrange and Euler-FCT domains are activated and the landmine detonated. As explained earlier, the detonated landmine was initially modeled as a circular disc-shaped high mass-density, high energy-density sub-domain within the lower Euler-FCT region.

A standard mesh sensitivity analysis is carried out in order to ensure that the results obtained are insensitive to the size of the cells used to represent the domains initially filled with the mine, soli and air. The effect of mesh size in various components of the vehicle was not explored.

III. RESULTS AND DISCUSSION

III.1 Mine-blast Induced Impulse Loading

The effect of mine blast on the target vehicle/structure is traditionally analyzed by replacing the interactions between the detonation products, the sand ejecta and the target with some form of simplified empirically-based loading function. Two of such functions that are most commonly used are: (a) CONWEP (Conventional Weapon) air-blast loading function [19] and (b) the loading function proposed by Westine et al. [20].

The CONWEP loading function was originally designed for use with a free-air or a ground-laid mine detonation. Neither of these two conditions accurately represents the situation encountered in the case of anti-vehicular mines which are typically buried in the soil to a depth of 5-20cm. Since the depth of burial of a mine can have a significant effect in directing the energy onto the target by funneling the force of the mine blast upwards and the sand ejecta play a major role in the momentum transfer to the target, the use of the CONWEP loading function in the analysis of the structural response of the vehicle/structure to the mine blast is expected to have a limited value.

To prescribe the CONWEP loading function, only the following details have to be provided for the explosive charge [19]: its mass, position and the TNT equivalent (the mass of TNT that would give the same blast performance as the unit mass of the explosive in question). This information is then used to compute the blast-loading pressure as a function of the radial distance from the charge center as:

$$P = P_r \cos^2 \theta + P_{in} \left(1 + \cos^2 \theta - 2 \cos \theta \right) \tag{32}$$

where P_r denotes the reflected (normal incident) pressure, P_{in} denotes the incident (side-on incidence) pressure and θ is the angle of incidence. The mathematical expressions for P_r and P_{in} (tenth order polynomials of the logarithm of the scaled radial distance, i.e. the radial distance divided by the TNT-equivalent charge weight) can be found in Ref. [19].

The loading function proposed by Westine et al. [20] was developed empirically by measuring the total impulse resulting from the explosion of a shallow-buried mine on a rigid plate with plugs. By measuring the initial velocity of the plugs, Westine et al. [20] developed the following relationship for the specific impulse, i_z:

$$i_Z = 0.1352 \left(\frac{\tanh(0.9589 P_s)}{P_s} \right)^{3.25} \frac{\rho_{soil}^{\frac{1}{2}} W^{\frac{1}{2}} \left(1 + \frac{7d}{9s}\right)}{s^{\frac{1}{2}}} \tag{33}$$

where

$$P_s = \frac{rd}{s^{\frac{5}{4}} A_{mine}^{\frac{3}{8}} \tanh\left(2.2 \frac{d}{s}\right)^{\frac{3}{2}}} \tag{34}$$

and r is the radial distance of a point on the target from the vertical line passing through the center of the mine, d is the depth of burial, A_{mine} is the area of the mine, s is the stand-off distance, W is the energy released by the mine and ρ_{soil} is the density of soil. It should be noted that s and d in Eq. (34) are measured with respect to the center of the mine. It is important also to note that the loading function was originally developed using 0.27kg shallow-buried mines. Thus, when the loading function of Westine et al. [20] is used to quantify the blast loading results from the detonation of anti-vehicle mines (6-10kg in mass); one assumes that the specific impulse scales linearly with the

mass of the mine. Some justification for this assumption was given by Morris [21]. Morris [21] further extended the loading function of Westine et al. [20] to include the effect of target inclination. The specific impulse equation proposed by Morris contains the Eq. (33) multiplied by a factor $\dfrac{\cos\theta}{\cos\beta}$, where θ is the angle between the target-plate normal and the line connecting the mine center with the point on the target, while, β is the angle between the vertical axis passing through the mine center and the line connecting the mine center to the same point on the target.

To demonstrate that the two blast-loading functions mentioned above cannot accurately account for the blast loading resulting from the detonation of a mine shallow-buried in soil, a simple target consisting of a number of concentric, unconnected rings (plus the central circular disk) are used in this section. The AUTODYN model parameters are as follows: the stand-off distance, 0.3m; the depth-of-burial, 0.1m; target thickness, 0.5m and ring width/disk radius of 4m. The initial location of the target and its location after 5ms for the case of dry soil are shown in Fig.3(a). A comparison of the radial distribution of the specific impulse transferred to the target obtained using the two blast loading functions and the AUTODYN calculations is shown in Fig.3(b). It is clear that the two blast-loading functions fail to accurately account for the magnitude, the radial distribution of the specific impulse transferred to the simple target in question as well as to account for the effect of moisture content in the sand. It is, hence, expected that their utility in the case of a more complex target like the Ford F800 series single-unit truck will be even more limited.

(a)
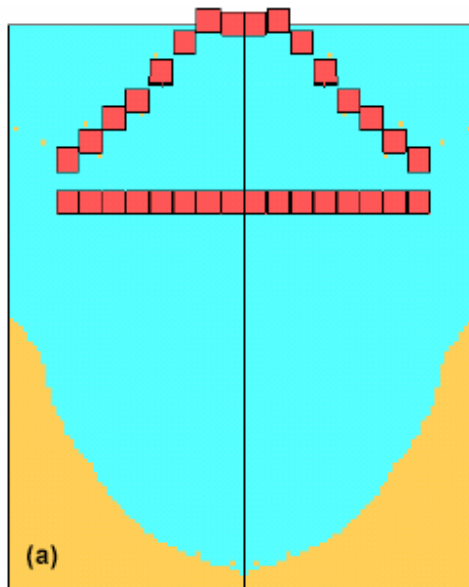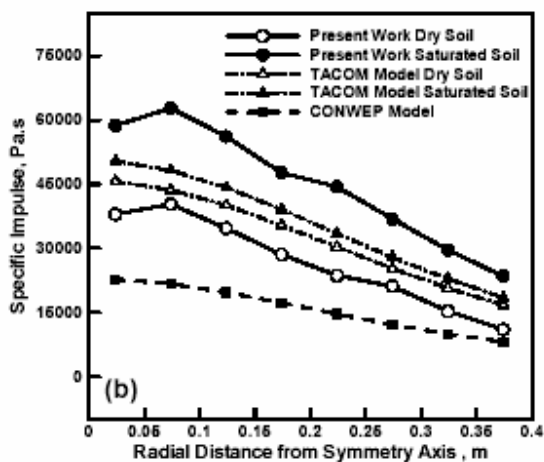
Fig.3 (a) Simple segmented-target model used to demonstrate deficiencies of the blast-loading functions; **(b)** A comparison of the resulting radially-dependent specific impulse.

III.2.The Role of Degree of Sand Saturation

The results displayed in Fig.3(b) clearly indicate that the extent of saturation of sand can play a significant role in affecting the magnitude of the mine-detonation induced momentum transfer to a target. It is clear that significantly higher momentum (scales with the area under the specific impulse vs. radial distance) is transferred in the case of saturated sand in comparison to that in the case of dry sand. Furthermore, the radial distribution of the specific impulse indicates that a tunneling effect (the blast loading associated with shallow buried mines is localized in the upward direction) is more pronounced in the case of saturated sand. To provide an explanation for these observations, a simple axi-symmetric transient non-linear dynamics analysis of landmine detonation in (a) dry sand (b) saturated sand is carried out using AUTODYN.

The results of this analysis pertaining to the temporal evolution of material deformation are shown respectively in Figs.4 and 5. A comparison of the results displayed in Figs.4 and 5 establishes two main differences between landmine detonations in dry sand and saturated sand: (a) the volume of the crater produced in the sand. (i.e. the volume of the ejected sand) is larger in the case of the saturated sand resulting in a higher momentum which can be transferred to the target; and (b)in the case of saturated sand the sand over burden bubble can undergo significantly more deformation before it fractures and allows venting of the gaseous detonation products. This in turn promotes the tunneling effect previously mentioned in conjunction with Fig. 3(b).

The observed differences in the magnitude and the spatial distribution of the detonation-induced specific impulse in the case of land mines shallow buried in dry sand and saturated sand can (as will be shown in next section) have a significant effect of the response of the target (F800 serves single-unit truck).

To further expose the differences between landmine detonation in dry and saturated sand, pressure vs. time data were analyzed at different points in the air above the sand with a detonating landmine. In general, the pressure vs. time traces show a zero overpressure (the pressure level in excess of the atmospheric pressure) up to the moment of arrival of the detonation products and sand ejecta, when it experiences a fast rise to a maximum value. The pressure then begins to drop at a longer relaxation time than the rise time. To better understand the nature of the impulse loading, a discrete Fourier analysis is next used to convert the pressure vs. time data to the frequency domain. This was done through the use of 2^n-point fast Fourier transform (FFT). Next, the corresponding power spectrum density plots were generated which revealed the energy content associated with the different frequency components. This procedure enabled identification of the main frequency components in original (pressure vs. time) signals. An example of the results obtained is given in Figs.6 (a)-(b). The results displayed in Fig. 6(a) were obtained at a point located at the vertical line passing through the center of the mine (standoff distance =0.6m) while the results displayed in Fig.6(b) were obtained at a point with the same standoff distance but with a radial offset of 0.35m. The results displayed in these figs. reveal that the blast loading associated with landmine detonation in saturated sand is dominated by frequency components lower than ~4Hz while frequency components upto ~15Hz are present in blast loading arising from landmine detonation in dry sand. As will be shown in the next section, these differences may be responsible for some of the observed differences in the kinematic response of the truck to landmine detonation in dry and saturated sand.
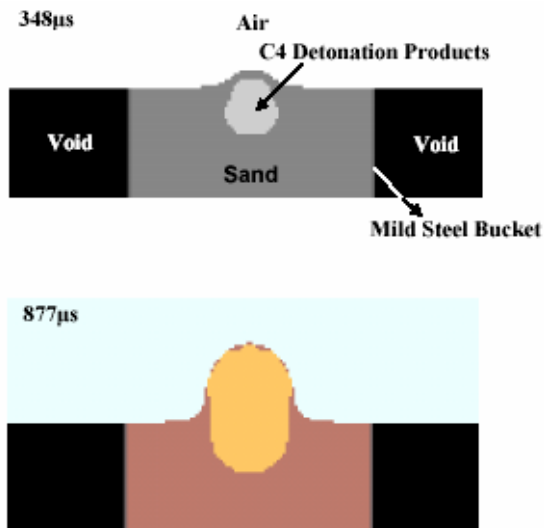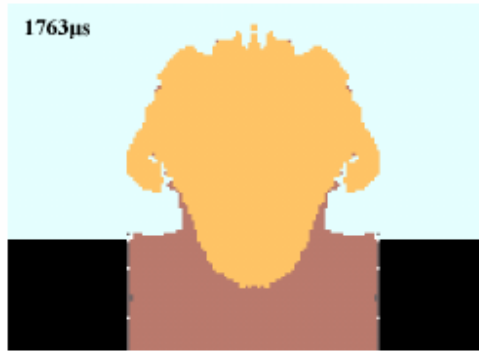
Fig.4 Temporal evolution of material deformation in the case of landmine detonation (DOB= 8cm) in the case of dry sand.
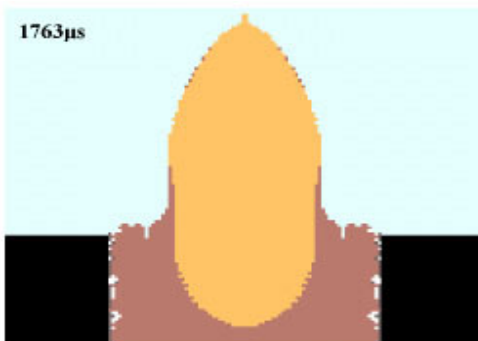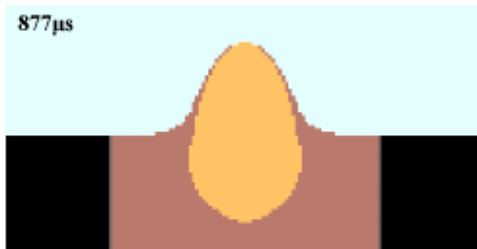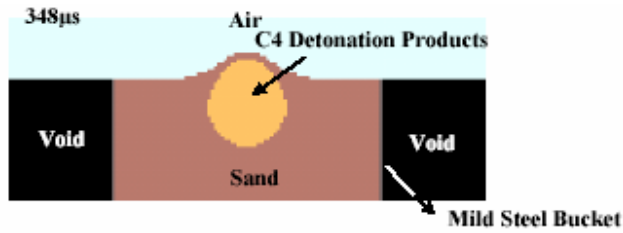

Fig.5 Temporal evolution of material deformation in the case of landmine detonation (DOB= 8cm) in the case of fully saturated sand.
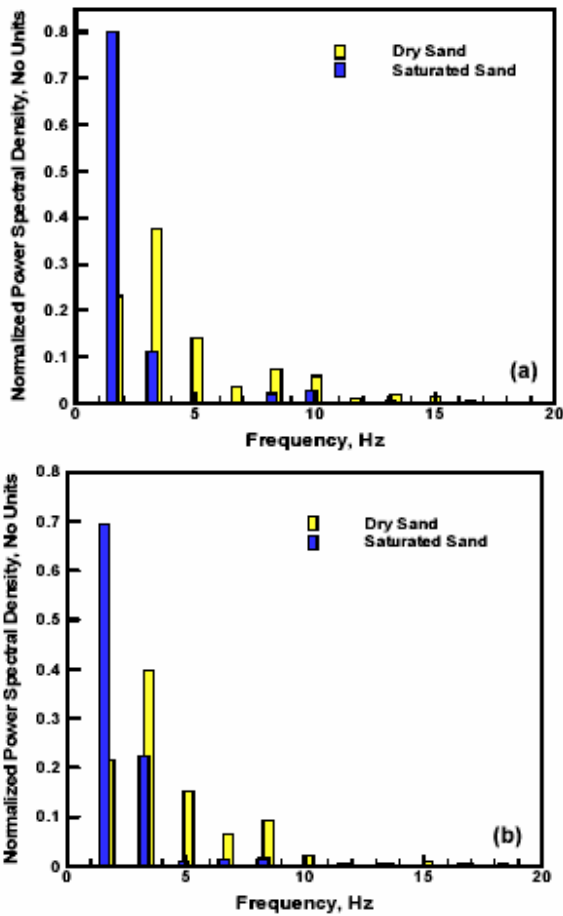
Fig.6 Typical results of the discrete Fourier analysis of the pressure vs. time signals associated with landmine detonation in dry and saturated sand; **(a)** a point lying on the vertical line passing through the center of the mine; and **(b)** a point located at a radial offset from the same line.

III.3. Response of the F800 Series Single-Unit Truck to Landmine Blast

In this section, selected results pertaining to the response of an F800 series single unit truck to a 7.5 kg C4 landmine blast under the truck's front right wheel are presented and discussed. All the results pertain to the case of a cylindrical mine (diameter=0.2m, height=0.1m) buried (in either the dry or saturated sand) to a depth of 0.1 m.

Figs.7 and 8 show the temporal evolution of the truck kinematics (including damage and failure) for the cases of landmine detonation in dry sand and saturated sand, respectively. It should be noted that, in order to display different features of the vehicle kinematics/damage, different view angles were used at different post-detonation times in Figs.7 and 8. The results displayed in these figs. reveal some clear differences in the

ballistic response of the vehicle, which are brought about by the differences in the moisture content of the sand. These differences can be summarized as follows:

(a) The kinematic response of the truck is, in the case of the landmine detonation in saturated sand, initially highly concentrated at the front-end of the vehicle, Fig.8(a), while in the case of the detonation in dry sand, the displacement field spreads over a larger area of the truck, Fig.7(a). This finding is clearly related to the previously mentioned blast tunneling effect which is more pronounced in the case of saturated sand;

(b) The total momentum transferred to the truck (roughly represented at a given post-detonation time by the magnitude of the vehicle translational and rotational motions and the extent of vehicle damage) is significantly higher in the case of the saturated-sand landmine detonation. This finding is also quite expected considering the results presented in Figs. 4 and 5 and the discussion presented in Section III.2;

(c) The initial response of the truck to the landmine detonation in saturated sand is completely dominated by torsion of its longitudinal beams and the deformation/damage of the vehicle's front end. In the case of dry sand landmine detonation, the kinematic response of the truck involves additional deformation modes. For example, upward bending of the engine support beams gives rise to a engine/hood contact and, in turn, to buckling of the hood, as can be clearly seen in Fig.8(b). While some explanation for these differences can be obtained by recognizing again the differences in blast-load spreading in the case of dry and saturated sand landmine detonation, additional justification will be provided later in this section; and

(d) Both in the case of landmine detonation in dry and saturated sand, the structural damage and failure are not that pronounced at the rear portion of the vehicle. This can be rationalized by the fact that even in the case of dry sand landmine detonation where the tunneling effect is not very pronounced, the direct impact of the vehicle by sand ejecta and gaseous detonation products takes place mainly in the front-end of the vehicle. Consequently, the load path to the rear end of the vehicle is primarily through the front end. Due to the blast nature of the loading and the finite stiffness of the vehicle's front end, the front end undergoes excessive plastic deformation, damage and failure (the phenomena that lead to stress relaxation) before the load reaches the rear end of the vehicle. As a result of this, the kinematic response of the rear-end of the vehicle is dominated by elastic deformations and rigid body motions.

To obtain a further insight into the differences in the kinematic response of the vehicle to landmine detonation in dry and saturated sand, the temporal evolution of (the magnitude of) the velocity at several points in the vehicle was monitored. The (time-domain) velocity signals were next processed using the 2^n-point FFT and, from the resulting power spectrum density plots, the main frequency components in the original (velocity vs. time) signals were identified. An example of the results obtained through the use of the aforementioned signal processing procedure is given in Figs. 9(a)-(b) for the cases of landmine detonation in dry and saturated sand, respectively. The results presented in Figs.9 (a)-(b) were obtained at two points located on the engine support cross member, one on the left and the other on the right side of the truck. A detailed analysis of the power spectral density plots at various locations in the vehicle (in addition to the ones displayed in Figs.9 (a)-(b)) showed that:

(a) In the case of saturated-sand landmine detonation, the velocity signal on both the front right and the front left sides of the vehicle is dominated by the frequency components roughly lower than 3.5 Hz; and

(b) In the case of dry-sand landmine detonation, both on the front right and the front left sides of the vehicle, the >5 Hz frequency components can be observed in the original velocity signal.

A further discussion of the differences in the power spectral density plots given in Figs.9 (a) and 9(b) is given later in this section after the results of an eigen-frequency analysis of the truck are presented.

To understand the failure modes of the vehicle, an analogy to linear response of discrete systems subjected to impulsive loading is drawn. A discrete dynamic system with multiple degrees of freedom subjected to pure impulse responds with the excitation of all its structural modes. The participation factor of each mode depends on where the impulse is applied and whether it deforms the system in a pattern similar to that of a particular mode. Hence it may be possible to tailor the damage to a vehicle under such a loading by tailoring the modal structure of the vehicle. A blast such as the one presented in this paper is expected to be a relatively broad band event in the frequency domain and hence is expected to excite a number of different modes in the vehicle. However in keeping with the earlier comment, the system's response is expected to be dominated by the mode that is closest to being excited due to the location of the blast. An eigen value analysis of the vehicle structure was therefore conducted and the eigen-modes and their corresponding eigen-frequencies were obtained using the Lanczos numerical eigen-solver [22]. The results are presented in Table 2.

The analysis shows the presence of structural modes in the lower frequency range, namely a torsional mode (about 2.5Hz) in which the cab and the trailor oscillate out of phase with each other as though connected by a torsional spring. Other modes of interest that are present include chassis horizontal and vertical bending modes and a hood mode as shown in Table 2. The point of application of the blast is under the front right tire of the vehicle. This point of application of the impulse is closest to exciting the chassis torsional mode of the vehicle described above. Hence the extensive response of the vehicle in this mode as showed in Figs.7 and 8. Further analysis of the frequency content of the pressure vs time signals from the two blasts show little energy content in the case of both dry and saturated past the 10 Hz range. In addition, especially for the saturated sand case, frequency content between 3 and 8 Hz is not observed while for the dry sand case significantly more energy content is observed in this range and upto 10Hz. This is corroborated through observation of the frequency content of the velocity signals on both the front right and the front left sides. A more pronounced hood buckling is observed in the case of dry-sad landmine detonation case again reflecting the higher energy content around 10 Hz. It is possible that the frame vertical bending mode could be excited but because of the dominant response of the torsional mode is not easily observed. The dominant failure mode in the vehicle for both cases is a torsional response in which the cab of the vehicle twists relative to the rear of the vehicle.

In the case of the saturated sand blast, energy content is concentrated at <3 Hz resulting in a much more violent response in the torsional mode. Such dynamic deflections contribute to excessive plastic deformation and promote damage initiation and failure in the vehicle components (Particularly in the ones which take part in the blast-excited vibrational modes of the vehicle).

(d)
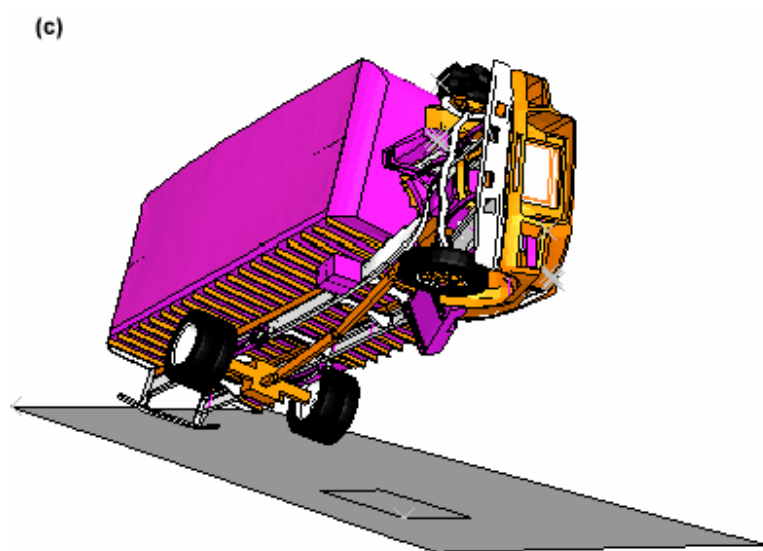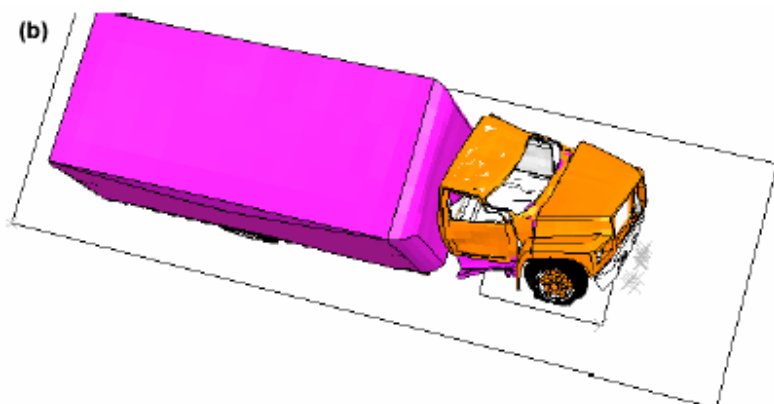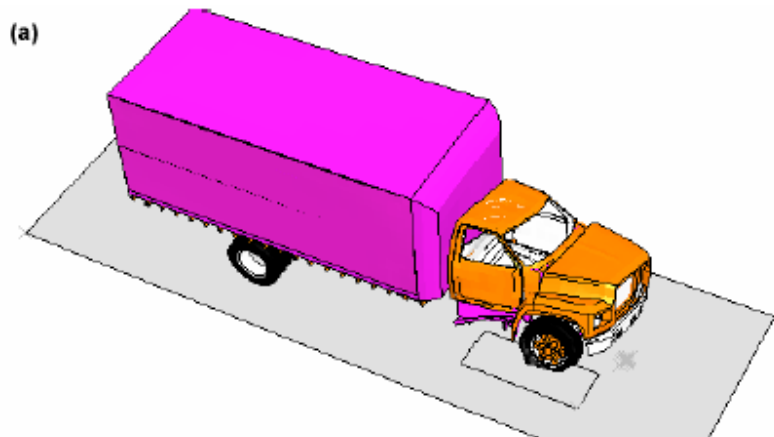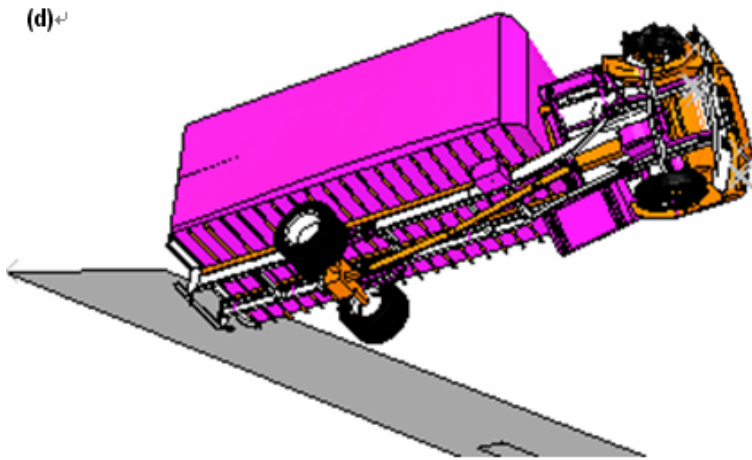
Fig.7 Temporal evolution of the kinematics/damage of the F800 series single unit truck following detonation of a 7.5kg C4 landmine buried to 10cm in dry sand below the front right tire: **(a)** t=0.08s; **(b)** t=0.14s; **(c)** t=0.35s and **(d)** t=0.45s.

(a)

(b)
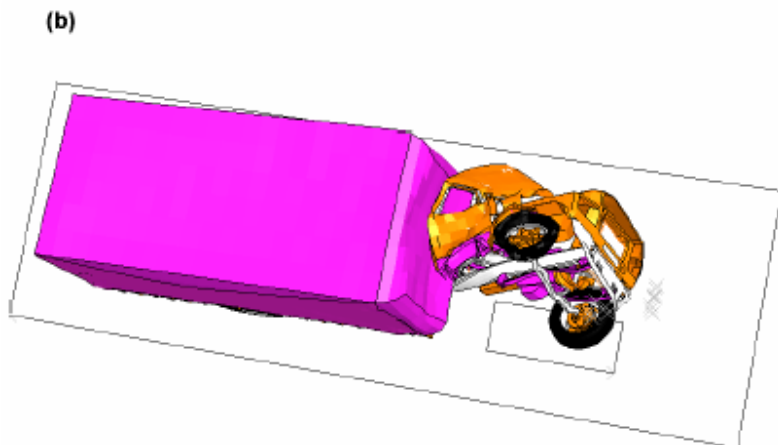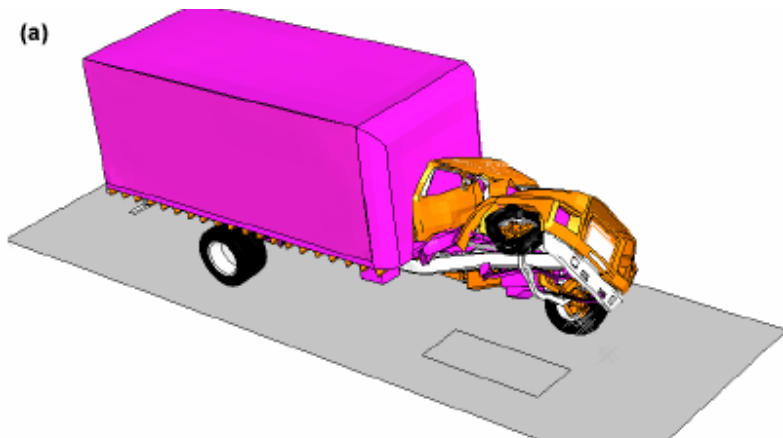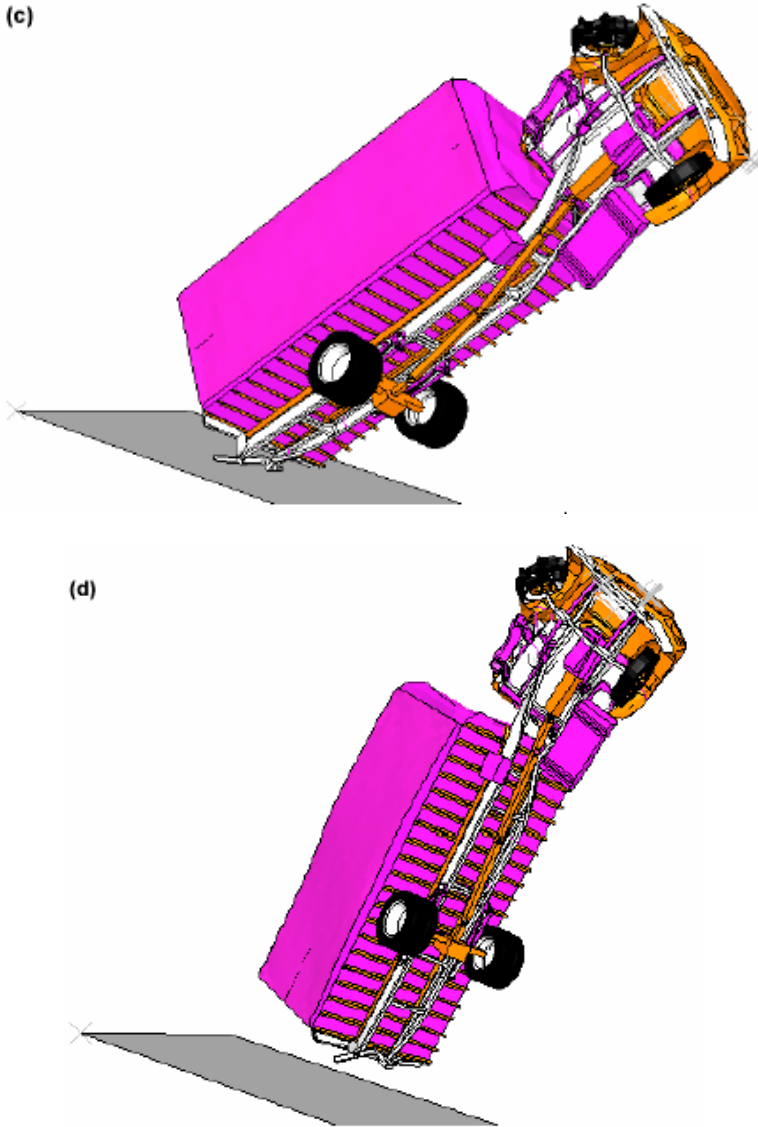
Fig.8 Temporal evolution of the kinematics/damage of the F800 series single unit truck following detonation of a 7.5kg C4 landmine buried to 10cm in saturated sand below the front right tire: **(a)** t=0.08s; **(b)** t=0.14s; **(c)** t=0.35s and **(d)** t=0.45s.

III.4. Computational Fluid Dynamics Aspects of the Present Work

The work discussed in the present work deals with the interactions of landmine detonation products, landmine fragments and sand ejecta with a commercial vehicle structure. Computational modeling of these interactions is carried out by combining a control-volume Euler formulation for the air and the gaseous detonation products with a

finite element formulation for the sand and the vehicle structure. In the previous section of the paper, a detailed analysis was given of the structural response of the vehicle to the landmine blast. To obtain a realistic response of the vehicle to the landmine blast, considerable effort was invested in developing realistic materials models and a realistic geometrical model for the vehicle components and assemblies. However, since the present work falls into a group of studies dealing with the fluid/solid interactions, the computational results are equally dependent on the way the Eulerian portion of the problem is dealt with. In this section, we address some of the key aspects of the Eulerian processor i.e. of the Computational Fluid Dynamics used in the present work.
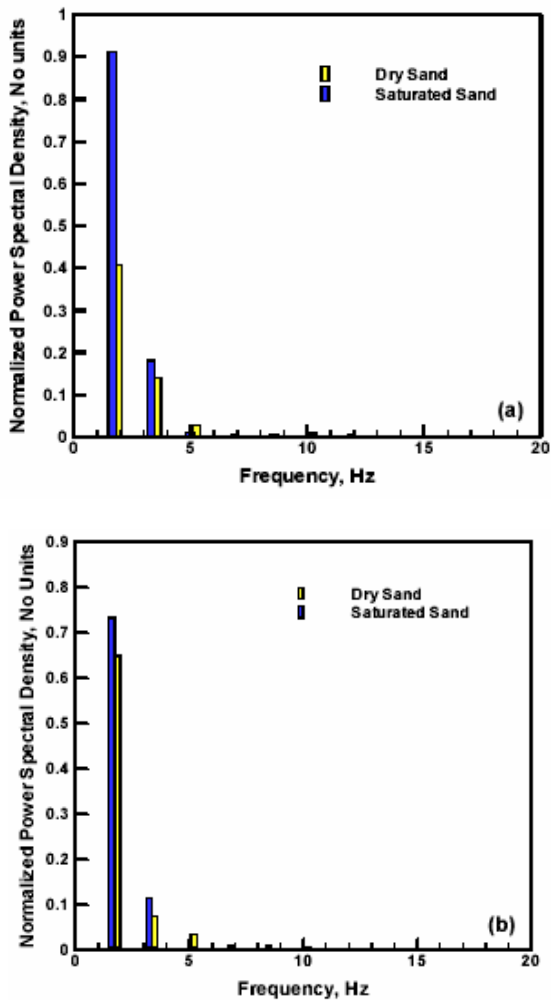

Fig.9 An example of the results of the truck local velocity vs. time signal processing analysis associated with landmine detonation in dry and saturated sand; **(a)** at a point located on the right hand side of the engine support cross beam; and **(b)** on the left hand side of the engine support cross beam.
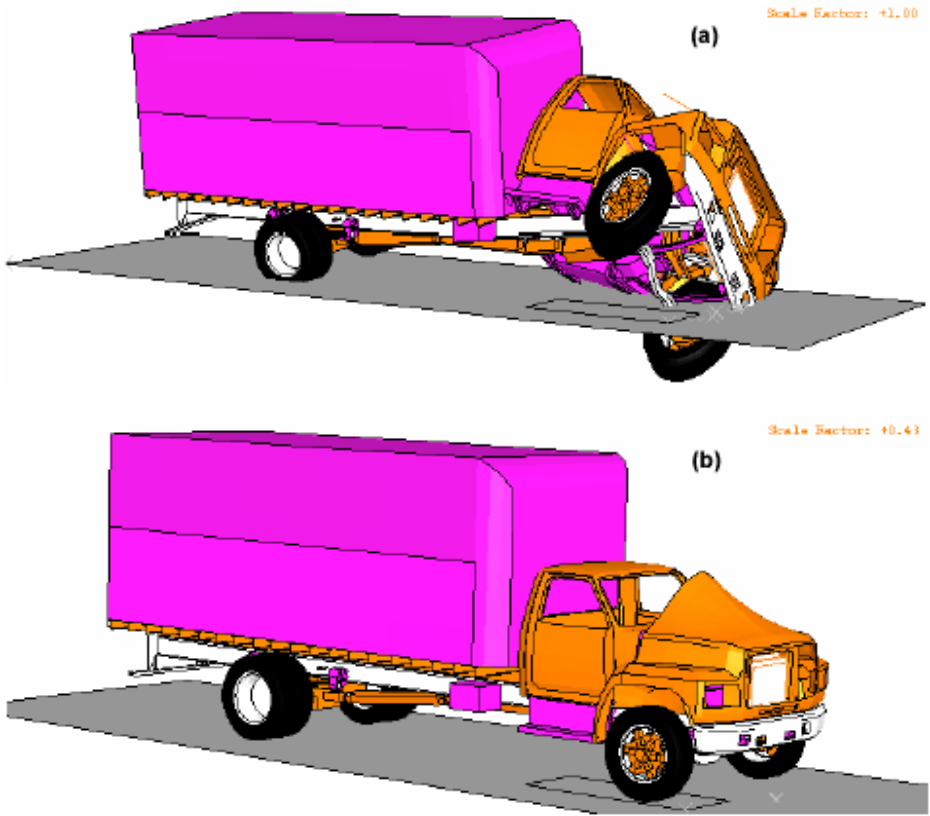
Fig.10 (a) The first torsional mode (eigen-frequency= 2.53Hz) and **(b)** the first hood-lid flexing mode (eigen-frequency= 8.09Hz).

As previously mentioned in Section II.2.2, a single material Euler FCT (Flux Corrected Transport) processor is used to represent air and gaseous detonation products. Due to the use of a single-material Euler-FCT processor for the gas-phase region, the landmine detonation products are not modeled as a separate material within the gas phase. Rather, the landmine detonation products are modeled initially as a cylindrically shaped air region with a high density ρ and a high internal energy density. Following Fairlie [13], the initial density of the detonation products is taken to be the density of the solid TNT explosive and the initial internal energy of this gas is determined by converting the value of the Chapman-Jouget internal energy per unit volume to the corresponding value of the internal energy per unit mass. The corresponding detonation products pressure and the fire ball temperature are computed using standard thermodynamic relations. Within the Euler-FCT processor the governing conservation (Navier Stokes) equations for a compressible inviscid flow are solved. While solving these equations the effect of turbulence is accounted for through the use of an artificial viscosity term whose magnitude is assessed via the application of the Monotonically Integrated Large Eddy Simulation (MILES) algorithm [23].

The interactions between the Euler and Lagrange processors are modeled by defining

the boundary conditions along the Euler/Lagrange interface in the following way. Along an Euler/Lagrange interface, the Lagrange region acts as a geometric boundary to the adjoining Euler region while the Euler region provides a pressure boundary to the Lagrange region. As the Lagrange region moves and distorts during calculation, it fills and empties the fixed-size Euler cells. To avoid the formation of extremely small Euler cells that could greatly reduce the computational time-step, such cells are automatically merged with larger neighbors.

All the results presented in the previous sections were obtained using fixed Euler cells with dimension 12mm X 25mm X 25mm. These dimensions were obtained as a compromise between minimization of the computational cost and the attainment of weak sensitivity of the results to further refinements in the cell size. In other words, a further refinement in the fixed-cell size Euler meshes was found to alter the key computational results by only a couple of percent.

IV. SUMMARY AND CONCLUSIONS

Based on the results obtained in the present work, the following main summary remarks and conclusions can be drawn:

1. The kinematic response of a soft-skinned vehicle (represented by a F800 series single-unit truck) to landmine detonation is very sensitive to the extent of (water) saturation of the sand into which the landmine is buried.

2. The amount of blast momentum transfer to the vehicle is substantially higher in the case of saturated-sand landmine detonation giving rise to significantly larger extents of the vehicle damage and rigid body motion.

3. Tunneling effect which focuses the shallow-buried mine blast loads in the upward direction (pronounced in the case of saturated sand) gives rise to the localization of the damage to the vehicle's front end. On the contrary, in the case of dry-sand landmine detonation, the damage is spread over a larger area of the vehicle.

4. The presence of the frequency components in the initial blast-loading impulse which match the vehicle's eigen-frequency appear to play a significant role in the kinematic response (including the effect of damage and failure) of the vehicle.

ACKNOWLEDGEMENTS

REFERENCES

[1].   J. E. Tremblay, D. M. Bergeron and R. Gonzalez, *"Protection of Soft-Skinned Vehicle Occupants from Landmine Blasts,"* The Technical Cooperation Program, Subcommittee on Conventional Weapons Technology, Technical panel W-1, Key Technical Activity 1-29, August 1998.

[2].   K. Williams, S. McClennan, R. Durocher, B. St-Jean and J. Tremblay, "Validation of a Loading Model for Simulating Blast Mine Effects on Armored Vehicles," *Proceedings of the 7th International LS-DYNA Users Conference,* Detroit, MI, 2002, 35-44.

[3].   K. Williams and K. Poon, "A Numerical Analysis of the Effect of Surrogate Anti-Tank Mine Blasts on the M113," *Report No. DREV TM-2000-007, Defense Research Establishment Valcartier*, Quebec, Canada, 2000.

[4].   M. Grujicic, B. Pandurangan and B. Cheeseman, "The Effect of Degree of Saturation of Sand on Detonation Phenomena Associated with Shallow-buried and Ground-laid Mines," *Shock Vib.*, 13(2006)41-61.

[5].   M. Grujicic, B. Pandurangan and B. Cheeseman, "A Computational Analysis of Detonation Phenomena Associated with Mines Shallow-buried in Sand," *Multidiscipline Model. Mater. Struct.*, accepted for publication, January 2006.

[6].   C. H. Tai, J. T. Teng, S. W. Lo, C. W. Liu, "A Numerical Study in the Interaction of Blast Wave with a Wheeled Armored Vehicle," *IJVD*, In press, 2006.

[7].   *AUTODYN-2D and 3D, Version 6.1, User Documentation*, Century Dynamics Inc., 2006.

[8].   M. Grujicic, B. Pandurangan, B. A. Cheeseman, W. N. Roy and R. R. Skaggs, "Impulse Loading Resulting from Shallow Buried Explosives in Water-saturated Sand," *J. Mater. Design Appl.*, submitted for publication, March 2006.

[9].   *http://www.ncac.gwu.edu/vml/models.html*

[10]. *P3/PATRAN User Manual, PDA Engineering,* Publication 903000, 1993.

[11]. J. Hallquist, *LS-DYNA Users Manual-Version 960*, Livermore Software Technology Corporation, Livermore, CA, 2001.

[12]. H. Schinke, "HPD, A PATRAN to LSDYNA Translator," FHWA/NHTSA, *National Crash Analysis Internal Report*, April 1995.

[13]. G. Fairlie and D. Bergeron, "Numerical Simulation of Mine Blast Loading on Structures," *Proceedings of the 17th Military Aspects of Blast Symposium*, Nevada, June 2002.

[14]. G. R. Johnson and W. H. Cook, "A Constitutive Model and Data for Metals Subjected to Large Strains, High Strain Rates and High Temperatures," *Proceedings of the 7th International Symposium on Ballistics*, 1983.

[15]. G. R. Johnson and W. H. Cook, "Fracture Characteristics of Three Metals Subjected to Various Strains, Strain Rates and Temperatures," *Eng. Fract.Mech.*, 21(1985)31-48.

[16]. P. J. Blatz and W. L. Ko, "Application of Finite Elasticity to the Deformation of Elastic Materials," *Transactions of the Society of Rheology*, 6(1962)227-251.

[17]. P. Laine and A. Sandvik, "Derivation of Mechanical Properties for Sand," *Proceedings of the 4th Asia-Pacific Conference on Shock and Impact Loads on Structures*, CI-Premier PTE LTD, Singapore, November 2001, 361-368.

[18]. S. Stein and T. Kim, "Effect of Moisture on Attraction Force on Beach Sand," *Mar.Geosource Geotec.,* 22(2004)33-47.

[19]. Glenn Randers-Pehrson and Bannister, K.A., "Airblast Model for DYNA2D and 3D," Army Research Laboratory, *Report: ARL-TR-1310*, Aberdeen Proving Ground, Maryland, 1997.

[20]. Westine, P.S, Morris, B.L., Cox, P.A and Polch, E.Z., "Development of Computer Programs for Floor Plate Response from Landmine Explosions," *Contract Report No. 13045 for U S Army*, TACOM research and Development Center, 1985.

[21]. B. L. Morris, "Analysis of Improved Crew Survivability in Light Weight Vehicles Subjected to Mine Blast, Volume 1- Technical Report," *SWRI Project No. 06-5095*, U.S. Army Belvoir Research and Development Center, Fort Belvoir, VA, 1993.

[22]. B. N. Parlett, *The Symmetric Eigenvalue Problem*, Prentice-Hall, Englewood Cliffs, New Jersey, 1980.

[23]. D. Kuzmin, R. Löhner, S.Turek, F. Grinstein and C. Fureby, *Flux-Corrected Transport Principles, Algorithms, and Applications*, Springer Berlin, Heidelberg, 2005.